In vitro interaction and biocompatibility of titanate nanotubes with microglial cells

S. Sruthi, A. Loiseau, J. Boudon, F. Sallem, Lionel Maurizi, P.V. Mohanan, G. Lizard, N. Millot

In vitro interaction and biocompatibility of titanate nanotubes with microglial cells

S. Sruthi[1,2], A. Loiseau[2], J. Boudon[2], F. Sallem[2], L. Maurizi[2], P.V. Mohanan[1], G. Lizard[3*], N. Millot[2*]

[1] *Toxicology Division, Biomedical Technology Wing, Sree Chitra Tirunal Institute for Medical Sciences and Technology, Thiruvananthapuram - 695 012, Kerala, India*

[2] *Nanosciences Department, Laboratoire Interdisciplinaire Carnot de Bourgogne, UMR 6303 CNRS/Université Bourgogne Franche-Comté, 9 av. A. Savary, BP 47 870, 21 078 Dijon, France*

[3] *Faculté des Sciences Gabriel, Laboratoire Bio-PeroxIL, EA7270, Université Bourgogne Franche-Comté / Inserm, 6, Bd Gabriel, 21000 Dijon, France*

*corresponding authors:

Nadine.Millot@u-bourgogne.fr and Gerard.Lizard@u-bourgogne.fr

Abstract

Titanate nanotubes (TiONts) are promising agents for biomedical applications. Microglial activation and associated oxidative burst are major challenges in drug delivery applications across the brain. Here, TiONts were designed for drug delivery systems by functionalizing them with (3-aminopropyl) triethoxysilane (APTES), their interactions and biocompatibility were studied *in vitro* using murine microglial BV-2 cells. TiONts-APTES exposure resulted in increased ROS production and transient mitochondrial hyperpolarization. However, there was

no indication of microglial proliferation in BV-2 cells as suggested by cell cycle analysis and cell count. The internalization process of TiONts-APTES into cells by endocytosis vesicles and passive diffusion were proved by transmission electron microscopy (TEM) with and without amiloride, the endocytosis inhibiting agent. In addition, the TiONts-APTES exhibited good biocompatibility on microglial BV-2 cells as revealed by the morphology and viability analysis.

Keywords: Titanate nanotubes; reactive oxygen species; microglial activation; mitochondrial hyperpolarisation; lysosomal integrity; apoptosis

Introduction

The central nervous system (CNS), comprising the brain and the spinal cord, is a highly protected organ, owing to the crucial functions it performs. Due to this fact, biomedical interventions in the brain are hard to achieve. Nanoparticles being very small in size can access otherwise protected sites in the body including blood brain barrier and placenta (Kessler, 2011). With the advancement of nanotechnology, many nanoparticles have been suggested as diagnostic and therapeutic modalities for neurobiological applications. Titanate nanotubes (TiONts) are one such particle with a needle-shaped morphology and surface chemistry (with hydroxides) which permit further functionalization (Papa *et al.*, 2015). Since their discovery by Kasuga *et al.* (1998), TiONts have been studied for a variety of applications (Bavykin and Walsh, 2010). Recently, applications of TiONts have turned to the biomedical field (Kijima, 2010) including dopamine detection (Niu *et al.*, 2008), DNA transfection (Papa *et al.*, 2013), bioimaging (Papa *et al.*, 2011), drug delivery (Loiseau *et al.*, 2017), and cancer cell radiosensitization (Mirjolet *et al.*, 2013, Mirjolet *et al.*, 2017).

TiONts have been proposed for glioma therapy (Mirjolet *et al.*, 2013) in addition to drug delivery and imaging applications (Boudon *et al.*, 2014). Moreover, it is

reported that TiONts can be used for the detection of neurotransmitters in the brain (Niu *et al.,* 2008). Though many neurobiological applications have been proposed for TiONts, only a little information is available on the biocompatibility and cellular interaction of these nanoparticles (Rihane *et al.,* 2016, Sallem *et al.*, 2017).

One of the main hurdles in the neuro-bio applications of nanoparticles includes nanoparticle-mediated microglial activation. Microglia are major immune cells of the brain which are involved in the scavenger functions and cytokine secretion. The activated microglia can induce oxidative stress in the brain which leads to further complications. In a recent study (Bussy *et al.*, 2015), it was reported that the carbon nanotubes toxicity mainly comes from the microglial activation and oxidative stress.

In the present study, TiONts were synthesized by hydrothermal synthesis and functionalized with APTES ((3-aminopropyl) triethoxysilane) for drug delivery applications. APTES functionalization provides TiONts with additional amine functions for drug molecule conjugation, making them better drug carriers. Moreover, APTES-functionalized TiONts exhibit better water dispersion and colloidal stability than bare TiONts. The interaction and biocompatibility of fully characterized TiONts-APTES with microglial cells were studied using microglial cells. BV-2 cell line was selected because it is derived from normal murine microglia and has phenotypic features similar to that of normal microglia (Blasi *et al.*, 1990). The toxicological responses including morphological alteration, reactive oxygen species (ROS) production, cell cycle alteration and cell death were studied using different bio-assays.

Methodology

Particle synthesis and characterization

Titanate nanotubes (TiONts) synthesis:

TiONts were prepared by a classical hydrothermal method in a basic medium (Papa *et al.*, 2009). TiO_2 rutile precursor powder (1 g) was added to a solution of NaOH (10 M, 250 mL). The mixture was ultrasonicated (30 min, 375 W, Sonics Vibra-Cells) and then transferred into a Teflon reactor with mechanical stirring and heating at 155 °C for 36 h. After cooling, the precipitate was centrifuged (24,000×g for 10 min), dialyzed four days (Cellu·Sep® tubular membranes of 12-14 kDa) and washed by ultrafiltration (regenerated cellulose membranes with a MWCO of 100 kDa) with deionized water until the conductivity reached 2 µS cm^{-1}. Finally, the TiONts were freeze dried.

Functionalization of TiONts with a stabilizing electrostatic agent (APTES):

Silane coupling agents present high reactivity with hydroxyl groups on the surface of metal oxide materials. Therefore, TiONts were modified with APTES (in large excess) *via* hydrolysis and condensation in a solution of water and ethanol (50:50 V:V) under magnetic stirring for 24 h to yield TiONts-APTES nanohybrids (Loiseau *et al.*, 2017). After the reaction, a part of the solvent was removed with a rotary evaporator (80 °C; 250 mbar) then the resulting suspension was ultrafiltered (100 kDa) to eliminate the unreacted APTES. Finally, TiONts-APTES were freeze-dried.

Nanoparticles characterization:

The TEM (Transmission Electron Microscopy) used was a JEOL JEM 2100

LaB6 microscope with an acceleration voltage of 200 kV and equipped with a high tilt pole-piece achieving a point-to-point resolution of 0.25 nm to study nanotube morphology and their agglomeration state. The samples were prepared by dropping a dilute suspension of powders on carbon-coated copper grids.

ThermoGravimetric Analysis (TGA, TA instrument, Discovery TGA) was used to determine the amount of grafted molecules on the surface of TiONts: water desorption and organic decomposition. The measurements were carried out under air atmosphere (25 mL min^{-1}) with a heating rate of 10 °C min^{-1} from 50°C to 800°C.

Specific surface area measurements were performed with a Micromeritics Tristar II apparatus and were calculated with the BET (Brunauer Emmett Teller) method (S_{BET}) from N_2 gas adsorption. Samples were first outgassed *in situ* under a pressure of 20 mTorr at 100°C (16 h) before N_2 adsorption/desorption cycles.

Zeta potentials (ζ-potentials) were measured with a Malvern Nano ZS instrument supplied by DTS Nano V7.11 software. The pH of the suspensions was adjusted from 3 to 11 by adding HCl or NaOH solutions. The Smoluchowski equation was used for zetametry measurements. For each measurement, powders were dispersed in 12 mL of aqueous NaCl solution (the final concentration of NaCl is 10^{-2} M). pH titrations were performed using aqueous solutions of HCl (0.1 M), NaOH (0.1 M), or NaOH (0.01 M).

UV-visible absorbance measurements were carried out using Shimadzu UV-2550 at 600 nm. Stability measurements were made in PBS 0.1 M at pH = 7.4 and T = 25°C (one measurement/5 min) during 120 min to analyze the colloidal stability.

The equipment of Fourier-Transform InfraRed spectroscopy (FT-IR) was a Bruker Vertex 70v using OPUS version 3.1. FT-IR spectra were obtained from

transmission measurements of thin pellets which consist of 2 mg of nanohybrids powder finely ground with dried KBr (198 mg) before being pressed into a pellet.

X-ray Photoelectron Spectroscopy (XPS) analyses were recorded by a PHI 5000 Versaprobe apparatus with a monochromatic Al $K_{\alpha 1}$ X-ray source (energy of 1486.7 eV with a 200 μm spot size, accelerating voltage of 12 kV, and power of 200 W). The resolution was 2.0 eV for global spectra and 1.3 eV for windows corresponding to selected lines. The powders were deposited on an indium sheet then pressed. Photoemission peak areas were calculated after subtracting background using a Shirley routine. The titanium 2p peak (458.7 eV) was used as reference and allowed the correction of charge effects. Gauss (70%)–Lorentz (30%) profiles were used and data were analyzed with CasaXPS software for curve fitting and MultiPak software for quantitative analysis.

Cell culture and nanoparticles treatment

The BV-2 cells were cultured in RPMI medium with 10% heat inactivated fetal calf serum (FCS) and antibiotic/antimycotic solution as previously described (Nury *et al.*, 2017). For the nano-interaction studies, cells were seeded in appropriate seeding density and cultured overnight. The cells were exposed to TiONts-APTES for different times (6 and 24 h) at concentrations of 1, 5, 10, 20, 40 and 80 µg/mL by diluting the stock solution (4 mg/mL).

Cytotoxicity and dose response: MTT assay

Cell viability was assessed as a function of mitochondrial activity using MTT (3-(4-,5-dimethylthiazol-2-yl)-2,5-diphenyltetrazolium bromide) assay. Cells were seeded in 12 well plates at an initial seeding density of 5×10^4 and incubated overnight at

37°C, 5% CO_2. After TiONts-APTES exposure, cells were harvested by centrifugation at 200×g for 5 min and then incubated with MTT (0.05 mg/mL) for 3 h in the dark. The formazan crystals formed were solubilized using 200 µL DMSO and absorbance was read at 540 nm. Final results are obtained by subtracting the absorbance of control wells (without cells) from the absorbance of treated samples in order to avoid nanoparticles interference in MTT results.

Cell morphology: Phase contrast microscopy

Cells were seeded in 12-well plates at an initial seeding density of 5×10^4 cells/well. Cells were exposed to TiONts-APTES for 24 h. Cellular morphology was assessed under a phase contrast microscope (Axiovert 40 CFL, Zeiss). Digital images were taken with an Axiocam ICm1 camera (Zeiss).

Particle uptake:

Flow cytometry

Uptake of TiONts-APTES by microglia was analyzed using flow cytometry following the method of Suzuki *et al*. (2007). Particle uptake by cells leads to an increase in granularity which is revealed by an increase in the side-scattered light (SSC), while the forward-scattered light (FSC) remains the same. In this experiment, cells were seeded in 6-well plates at an initial density of 1×10^5 and kept overnight for incubation. Cells were then exposed to 5, 20, and 80 µg/mL of TiONts-APTES for 6 h. Cells, harvested by centrifugation, were resuspended in 500 µL PBS and analyzed by flow cytometry using a Dako/Partec/GALAXY flow cytometer (Partec, Münster, Germany) equipped with a solid blue laser (50 mW) and controlled by 'FloMax' software (version 2.4; Partec).

Transmission electron microscopy (TEM):

The mechanism of nanoparticles uptake by BV-2 cells was studied using TEM. The cells were seeded at an initial density of 1.175×10^5/mL and incubated overnight. Cells were subsequently exposed to 20 µg/mL of TiONts-APTES for 24 h without and with 100 µM amiloride, a macropinocytosis inhibitor (added 1h prior to nanoparticles exposure). At the end of treatment, cells were harvested and fixed for 1 h at 4 °C in 4% paraformaldehyde and 2.5% of glutaraldehyde in Sorensen phosphate buffer (0.1 mM, pH 7.3). After fixation, samples were washed by Sorensen phosphate buffer. The post-fixation treatment was realized with 1% osmium tetraoxide at room temperature for 1h. Dehydration and resin impregnation of the samples were performed with a Leica EM AMW automatic microwave tissue processor: dehydration was done by increasing degrees of ethyl alcohol (50°, 70°, 95°, 100°), the substitution of ethanol by resin was progressively done by three absolute ethanol/Embed-812 resin mixtures (¾, ½, ⅓ ethanol), followed by two impregnations in pure Embed-812 resin. The polymerization of samples was performed with a mixture Embed-812/3% benzyldimethylamine (BDMA, polymerisation catalyst) in gelatin capsule maintained for 48 h at 60 °C. Blocks were cut on a Reichert ultramicrotome and slices (thickness of 70 nm) were deposited on copper and palladium grid. After drying, grids were contrasted with uranyl acetate and lead citrate. TEM observations of cells were realized on a HITACHI H-7500 operating at 80 kV. For each test carried out, one grid per sample was observed, which corresponds to a total of 30 to 50 cells. The photos presented are representative of the cells observed by samples.

Reactive oxygen species analysis

Superoxide radicals: DHE probe

Superoxide anions production in presence of TiONts-APTES was measured using a cell permeable molecule, dihydroethidium (DHE; Life Technologies, St Aubin, France). DHE, mainly upon reaction with superoxide anions ($O_2^{\bullet -}$), forms a red fluorescent product, 2-hydroxyethidium, which intercalates with DNA. The cells were seeded in 12-well plates at a density of 5×10^4 cells/well and kept overnight in the CO_2 incubator. After TiONts-APTES exposure, the cells were harvested by centrifugation. The pellets were resuspended in 1 mL PBS containing 1.6 mM DHE and incubated for 15 min at 37°C. The cells were analyzed by Dako/Partec/GALAXY flow cytometer (Partec) through a 590/10 nm band pass filter.

Peroxide radicals: DHR123 probe

Hydrogen peroxide production in the presence of TiONts-APTES was estimated using dihydrorhodamine 123 (DHR123, Sigma-Aldrich, USA). DHR 123 is an uncharged and non-fluorescent molecule that can passively diffuse across plasma membranes where it is oxidized to cationic rhodamine 123 by hydrogen peroxide (H_2O_2) to give green fluorescence. The cells were seeded on 24 well plates at an initial density of 2×10^4 cells/well and exposed to 5, 20, 40 and 80 µg/mL of TiONts-APTES for 6 and 24 h. The cells were harvested after centrifugation and resuspended in 1 mL PBS. 2mM DHR123 were added to each tube at a final concentration of 6 µM and incubated for 15 min at 37°C. Fluorescence were measured using Dako/Partec/GALAXY flow cytometer (Partec) with a 520/20 nm band pass filter.

Transmembrane mitochondrial potential (ΔΨm): $DiOC_6(3)$ probe

Alteration in transmembrane mitochondrial potential (ΔΨm) was analyzed using a fluorescent probe: 3,3'-dihexyloxacarbocyanine iodide ($DiOC_6(3)$ (Life Technologies, Molecular Probes). $DiOC_6(3)$ is a cell-permeant, green-fluorescent, lipophilic dye, which is selective for the mitochondria of live cells when used at a nanomolar concentration. $DiOC_6(3)$ allows measuring ΔΨm. The cells were seeded at an initial density of 2×10^4 cells/well of 24 well plates and incubated overnight. They were exposed to TiONts-APTES of concentration 1, 10, 20, 40 and 80 µg/mL for 6 h and 24 h. Cells incubated with 4% paraformaldehyde (in DPBS for 10 min at 37 °C) were used as positive control. The cells washed in PBS were incubated with $DIOC_6(3)$ (0.1 µM in PBS) for 15 min at 37°C. The flow cytometry analysis was done using the DAKO/GALAXY flow cytometer (Partec, Germany) with a 520/20 nm band pass filter.

Lysosomal membrane integrity: Acridine orange staining

Lysosomal destabilization in presence of nanoparticles was analyzed using acridine orange (AO). AO is a lipophilic, cationic and metachromatic fluorochrome capable of permeating cells and organelle membrane structure. Under a blue light excitation, the dye differentially stains cytoplasm and acid vesicles (Pierzyńska-Mach *et al.*, 2014). In normal cells, the dye gets protonated inside acidic vesicles and emits orange fluorescence whereas the cytoplasm remains green in color. When the cells have altered lysosomes, leading to an alteration of the proton pump, the resulting alkalinisation of the lysosomes is associated with a green/yellow fluorescence of these vesicles. The cells, seeded at an initial density of 2×10^4 cells/well of 24 well plates, were exposed to TiONts-APTES (5, 20, 40, and 80 µg/mL) for 6 h and 24 h. The cells, harvested by direct pipetting, were washed with PBS and incubated in 1 mL AO

solution (2 µg/mL in PBS) for 15 min at 37°C. The analysis was carried out using a Dako/Partec/ GALAXY flow cytometer (Partec) with a 590/10 nm band pass filter.

Plasma membrane integrity: Propidium Iodide (PI) staining

The plasma membrane integrity on TiONts-APTES exposure was analyzed by Propidium Iodide (PI) staining. The principle underlying the PI staining is dye exclusion by living cells (Lizard *et al.*, 1995). Cells seeded at an initial density of 2×10^4 cells/well of 24 well plates were exposed to TiONts-APTES (5, 20, 40, and 80 µg/mL) for 6 and 24 h. Harvested cells were washed and stained with PI (1 µg/mL) for 15 min at 37°C. The flow cytometry analysis was done using Dako/Partec/GALAXY flow cytometer (Partec) with a 630 nm long pass filter.

Poly(ADP-ribose) polymerase (PARP) cleavage assay

The cells were seeded at an initial density of 2×10^4 cells/well of 24 well plates and incubated overnight. The cells were exposed to 20 µg/mL and 80 µg/mL of TiONts-APTES for 24 h. Untreated cells were used as control. After treatment cells were harvested and centrifuged at 200×g, 4°C for 5 min.

Sample lysis and protein quantification

The cell pellets were transferred to fresh tubes and washed with 1 mL cold PBS. After discarding supernatant, the pellets were incubated with 80 µL of RIPA buffer containing 1× anti-protease for 30 min on ice. The cell suspension was centrifuged at 12,000×g for 20 min at 4°C. Supernatant was collected in a fresh tube (this solution can be stored at -20°C for weeks and thawed at room temperature) and the pellet was discarded. The concentration of protein solution was measured by BCA (Bicinchoninic

acid assay) with 2% copper sulfate solution. 25 µL of BSA was used as protein standard and concentration was calculated from the standard graph obtained.

Loading and running gel

The isolated protein was loaded in 8% polyacrylamide gel at a concentration of 70 µg/well. Electrophoresis was carried out for 2h (30 min at 70 V followed by 1.5 h at 120 V).

Gel to membrane transfer of protein

The polyvinylidene difluoride (PVDF) membrane was activated with methanol for 1 min and rinsed with transfer buffer. Gel stack was prepared by sandwiching the gel and PVDF membrane between filter papers and sponges and keeping them in transfer buffer for 1 h.

Antibody revelation by chemiluminescence

The protein attached membrane was blocked using 5% milk solution for 1 h at room temperature and washed 3 times with PBST (PBS and Tween 20, 0.1%) for 5 min each. It was transferred into a solution containing primary antibody (1:1,000) and incubated overnight at 4°C. Antibody for actin (1: 10,000) was used as a standard. The solution was washed 5 times with PBST (5 min each). The membrane was then incubated with secondary antibody (in 1% milk) for 1 h at 25°C and covered in a transparent plastic wrap after removing excess reagent. The image was acquired by chemiluminescence method.

Cell cycle analysis: propidium iodide staining

The changes in cell cycle patterns were analyzed by staining with propidium iodide (PI) (Marel *et al.*, 2008). In brief, the cells were seeded at an initial density of 2×10^4 cells/well on 24 well plates and exposed to TiONts-APTES (5, 20, 40, and 80 µg/mL) for 24 h. Cells, harvested by direct pipetting, were washed with PBS. The pellets were fixed using 1 mL cold 80% ethanol (kept at -20°C), by vortexing, to avoid cell aggregation and kept at -20°C for at least 2 h (cells can be kept in this condition for few days.). The cells were washed (350×g for 5 min) and resuspended in 300 µL PBS containing 80 µg/mL PI and 200 µg/mL RNase. After 1h incubation at 37°C, the solution was made up to 1 mL by adding 700 µL PBS and analyzed using flow cytometry on a Dako/Partec/GALAXY flow cytometer (Partec) with a 630nm long pass filter.

Statistical analysis

All the experiments were done in triplicates and the values were expressed as mean ± SD. Statistical comparison between the control and experimental values were done using one-way ANOVA test. In result, analyses with $p<0.05$ were considered as statistically significant.

Results

Nanotubes synthesis, functionalization, and characterizations

TEM images were used to highlight the synthesis of TiONts after the hydrothermal treatment. They present a spiral-shaped morphology, with internal cavity (Figure 1a,b) and a high specific surface area (S_{BET} = 174 ± 1 m^2 g^{-1}). They are (10 ± 1)

nm in outer diameter and (170 ± 50) nm in length.

The functionalization of TiONts with APTES (Figure 1e,f) seems to reduce nanoparticles agglomeration and improve their dispersion in comparison to bare TiONts (Figure 1c,d). The grafting ratio of APTES on the surface of TiONts was determined by TGA (Figure 2). The amount of hydroxyl groups on the surface of bare TiONts was calculated based on water weight loss from TGA curve. Indeed, the release of one molecule of chemisorbed water involves the condensation of two hydroxyl groups. As the weight loss below 175°C is due to physisorbed water (Sabzi *et al.*, 2009), only the weight loss related to chemisorbed water between 175 °C and 800 °C is taken into account for hydroxyl and grafting ratio estimation. Consequently, a greater weight loss is obtained after APTES grafting (Figure 2 and Table 1). The results show a hydroxyl density of about (10.6 ± 1.5) $OH.nm^{-2}$ and APTES grafting ratio of (7.3 ± 0.5) $APTES.nm^{-2}$. It should be noted that the specific surface area of TiONts decreases after their functionalization with APTES (S_{BET} = 147 ± 2 m^2 g^{-1}). APTES may form an envelope all around TiONts and hinder, at least partially, access to internal cavities.

ζ-potential measurements of TiONts-APTES indicated an isoelectric point (IEP) at pH 8.5 (Figure 3). This value is greater than that of bare TiONts (IEP at pH 3.3) due to the presence of amine functions (Paris *et al.*, 2015). Moreover, an inversion in ζ-potential sign is also observed at physiological pH, where it is positive *ca*. + 10 mV for APTES-functionalized TiONts and largely negative (*ca*. –25 mV) for bare TiONts.

X-ray Photoelectron Spectroscopy (XPS) analyses are realized to evaluate the chemical composition of the surface of TiONts-APTES. Besides to the chemical elements that are present in bare TiONts, some additional specific elements, such as nitrogen and silicon, are also found in TiONts-APTES (Table 2), thus proving the presence of APTES at the surface of nanotubes.

The FT-IR spectrum of TiONts-APTES proves the grafting of APTES molecule onto the surface of TiONts (Figure 4). APTES characteristic bands are located at 1000 cm^{-1} (ν Si-O-Si), 1100 - 1200 cm^{-1} (ν C-N) and 3250 cm^{-1} (ν NH_2).

Cytotoxicity and dose response: MTT assay

After 6 h, the exposure to TiONts-APTES does not markedly alter cells viability, which is evaluated with the MTT assay by measuring the activity of succinate dehydrogenase, except for 80 µg/mL treated wells. A statistically significant increase in absorbance (% control) is observed for 80 µg/mL treated samples at 6h of exposure which subsided by 24h. The absorbance is significantly reduced in 20 (93. 80 ± 5.84 %), 40 (90.12 ± 4.17 %) and 80 (84.24 ± 4.12 %) µg/mL TiONts-APTES treated wells at 24 h of incubation (Figure 5a).

Cell morphology

The cellular morphology in presence of TiONts-APTES is evaluated using a phase contrast microscopy. The treated cells do not show any alteration in their morphology like membrane rupture, swelling, blebbing and/or cytoplasmic disintegration which are morphological features usually associated to cytotoxic effects. The cells size and morphology are similar to those of the negative control cells (Figure 6a).

Particle uptake

TiONts-APTES uptake by BV-2 cells is analyzed from the SSC changes in flow cytometry. As shown in Figure 6b the TiONts-APTES exposed cells exhibit a dose-dependent increase in SSC (5 µg/mL: 5.04% and 80 µg/mL: 35%) compared to negative

(2.56%) and positive controls (12.5%) suggesting an internalization and/or an interaction of nanoparticles with the plasma membrane.

To define whether the nanoparticles were internalized and to determine by which mechanism – the passive (diffusion through the plasma membrane) or the active one (endocytose) – they can accumulate inside the cells, the nanoparticles uptake was studied by TEM. Cells are incubated with TiONts-APTES (20 µg/mL, 24 h), without and with amiloride (100 µM), an endocytosis inhibiting molecule introduced in the culture medium 1 h before nanoparticles (Figure 7). In TiONts-APTES-treated cells, the presence of nanoparticles was revealed in large vesicles (average diameters of the vesicles: 0.85 ± 0.32 µm) in all the observed cells (Figure 7b,b1,b2). However, when BV-2 cells were cultured with amiloride, only few cells with internalized nanoparticles (around 10 %) were found: this data supports TiONts-APTES internalization mainly by endocytosis (Figure 7c,c1). In these conditions, the interactions of nanoparticles with the plasma membrane are however observed, and their diffusion through the plasma membrane are detected (Figure 7c2,c3,c4). It is noteworthy that the size of the endocytic vesicles in amiloride-treated cells (0.50 ± 0.16 µm) are smaller than those in cells treated with nanoparticles only. Altogether, these data support that nanoparticles enter in cells mainly by endocytosis and show that a passive diffusion does exist. In the latter case, more individualized TiONts are observed into the cytoplasm and some of them are closer to nucleus.

On the other hand, a change in the mitochondrial behavior is observed in cells uptaking nanoparticles. Indeed, in the control cells, mitochondria are usually situated near to nucleus, in the majority of cells, however, in contact with TiONts-APTES, many mitochondria are located near the cellular membrane (Figure c2) or near the endocytic vesicles containing nanoparticles (Figure d,e). In addition, bigger mitochondria are

observed in nanoparticles-treated cells (0.94±0.57 µm) compared to control (0.64±0.29 µm). This change in mitochondrial size could be induced by the presence of TiONts-APTES nanoparticles and may affect the mitochondrial function.

ROS overproduction

Superoxide radicals

Superoxide anion production in the presence of TiONts-APTES is studied using the probe DHE. The cells exhibited a concentration dependent increase in DHE fluorescence at 6h of incubation. However, at 24h of treatment the particular trend was not observed in the treated wells, where the percentage of cells exhibiting DHE fluorescence declined. No concentration dependent increase in DHE positive cells were observed at 24h except for 80 µg/mL TiONts-APTES (Figure 8a).

Hydrogen Peroxide

Hydrogen peroxide production in the presence of TiONts-APTES is studied using the probe DHR 123 which is a cellular indicator of peroxides and peroxynitrite production. The results obtained shows little increase in the percentage of cells overproducing peroxide radicals' at 6 h except for the highest concentration of TiONts-APTES (80 µg/mL) (Figure 8a). Cells treated with 80µg/mL showed statistically significant increase in peroxide radical production at 6h. On the other hand, TiONts-APTES exposure at 24h showed a concentration-dependent and statistically significant increase in peroxides production (Figure 8b).

Transmembrane mitochondrial potential (ΔΨm)

A possible ΔΨm change in response to TiONts-APTES is evaluated using fluorescent probe $DiOC_6(3)$. Cells exhibit an initial mitochondrial hyperpolarization after 6 h of exposure, as revealed by the increase in the green intensity of $DiOC_6(3)$. 7-ketocholesterol (7-kc)-treated cells (positive control) also exhibits similar response. However, after 24 h, the ΔΨm in treated cells reverts to normal state and becomes similar to controls (Figure 9).

Lysosomal membrane integrity

Lysosomal membrane integrity in the presence of TiONts-APTES is analyzed by staining with acridine orange (AO). Flow cytometry analysis of AO stained cells does not indicate any signs of lysosomal membrane permeabilization (LMP) in TiONts-APTES-treated cells. AO signals increase in the treated cells for both 6 and 24 h suggesting the absence of TiONts-APTES mediated LMP in BV-2 cells (Figure 10).

Plasma membrane integrity

Plasma membrane integrity in the presence of TiONts-APTES is analyzed using PI staining. Flow cytometry analysis of the PI stained cells indicates no significant increase in the PI positive cells for 24 h with respect to control. As shown in Figure 11, cells treated with 80 µg/mL of TiONts-APTES show only 4.5% PI positive cells compared to 65.5% PI positive cells in 7-kc treated wells (positive control).

Mechanism of cell death

PARP cleavage assay is carried out to study the mechanism of TiONts-APTES mediated cell death in BV-2 cells. The little cells death observed in the present study is

407 *via* apoptosis as evidenced by PARP cleavage assay. A light band of cleaved PARP
408 could be visible in both 20 and 80 µg/mL of TiONts-APTES treated cells at 24h (Figure
409 12).

410 ***Cell cycle analysis***

411 TiONts-APTES mediated cell cycle changes are evaluated by staining the cells
412 with PI. The flow cytometry analysis of PI-stained cells indicates no alteration in cell
413 cycle pattern in the presence of TiONts-APTES. Moreover, SubG1 population
414 indicative of apoptotic cells (Ormerod *et al.*, 1992) are not visible in TiONts-APTES
415 treated cells for 24 h of incubation (Figure 13).

416 **Discussion**

417 TiONts have been proposed for a variety of biomedical applications including
418 drug delivery, bioimaging, cancer therapy, biosensing and disease diagnosis (Papa *et*
419 *al.*, 2011, Mirjolet *et al.*, 2013, Papa *et al.*, 2013, Boudon *et al.*, 2014, Loiseau *et al.*,
420 2017, Mirjolet *et al.*, 2017). TiONts are ideal candidates for neuro-bio applications
421 because of their low toxicity. In the present study, TiONts-APTES nanoparticles,
422 synthesized for drug delivery applications across BBB, are evaluated for their toxicity
423 using microglial cells line BV-2.

424 APTES grafting onto TiONts surface is confirmed by several chemical
425 characterization techniques such as zeta potential measurement, XPS and IR
426 spectroscopy. Indeed, the increase in the zeta potential value and the isoelectric point
427 after APTES grafting prove the presence of positively charged functional group on the
428 surface (amine groups). The increase in carbon percentage and the appearance of new
429 chemical elements such as nitrogen and silicon, observed by XPS analysis, confirm the

APTES grafting. Moreover, IR spectroscopy shows the characteristic vibration bands of APTES in TiONts-APTES spectrum. The grafting density of this molecule is estimated by thermogravimetric analysis to (7.3 ± 0.5) APTES/nm^2 of nanotubes, based on the difference in the weight losses between bare and grafted TiONts.

Cytotoxicity and dose response are studied in terms of mitochondrial activity by MTT assay. The mitochondrion is a highly sensitive organelle and hence early stage changes in the cellular health are reflected in mitochondrial activity. Dose-dependent alteration in mitochondrial activity after cells exposure to TiONts has been reported in some studies (Iavicoli *et al.*, 2011). Despite the change in mitochondria location and morphology observed in the present study through TEM images, no marked reduction in mitochondrial activity is observed after TiONts-APTES exposure. The statistically significant reduction observed in the mitochondrial activities are not beyond 30% to be called as cytotoxic according to the ISO 10993-5 guidelines for the *in vitro* cytotoxicity evaluation of medical devices. It is reported that TiO_2 nanoparticles interfere with MTT to give false positive results (Lupu and Popescu, 2013). In the present study, absorbance values of controls (without cells) are subtracted from the MTT results to rule out nanoparticles interference.

MTT results are just an indicator of cell metabolic state. Changes in MTT signals can be due to a cytotoxic effect, a cytostatic effect (Riss *et al.*, 2016) or to a loss of cells during the assay procedure. Therefore it is important to correlate the MTT results with cellular morphology and total cell count (Quent *et al.*, 2010). For this reason, Trypan blue exclusion assay is carried out to count the cells (data not shown here). In the present study, even high concentrations of TiONts-APTES does not elicit any morphological alteration or reduction in cell size or density after 24 h of exposure. It can be concluded from the obtained results, that the decrease in mitochondrial

activity, observed in MTT assay, cannot be due to the cytotoxic effect of TiONts-APTES. It is reported that TiO_2 nanoparticles induce size reduction and morphological alterations in cells (Saquib *et al.*, 2012). However, it is shown in the current result that TiONts-APTES do not elicit any morphological alterations in BV-2 cells.

Cellular uptake of nanoparticles is an important event in bio-nano interaction. Drug delivery applications require nanoparticles internalization. Moreover, the low toxicity, indicated in nanotoxicological studies, can be due to the failure of cells to internalize particles. In the present study cellular internalization of TiONts-APTES is proved by SSC granularity measurements and TEM observations. On the one hand, the dose dependent increase in SSC indicates nanohybrids uptake by BV-2 cells. Indeed, the results of the current study are in corroboration with those of Chen *et al*. (2010) where cellular internalization of TiO_2 nanorods was shown. As the increase in SSC may be also the result of apoptotic vesicles increase, the cells are exposed to a cytotoxic agent, 7-kc, to differentiate if the observed increase in granularity is due to TiONts-APTES uptake or apoptosis. The SSC changes in 7-kc treated cells are not as pronounced as those observed for TiONts-APTES which confirms the latter's uptake by BV-2 cells. On the other hand, TEM images confirm the internalization of TiONts-APTES and show two uptake processes; the first and main one is endocytosis process which is a dynamic internalization way, and during which the nanoparticles uptake is carried out by endocytic vesicles. The second and less probable process is the internalization of individualized nanotubes by passive diffusion through the cellular membrane. The latter mechanism is observed when the endocytosis phenomenon is inhibited with amiloride. This molecule is also used by (Huerta-Garcia *et al.*,2015*)* to illustrate the TiO_2 nanoparticles internalization by macropinocytosis for glial cells. It has been chosen because macropinocytosis is the main internalization pathway of

480 “large” objects (Benmerah and Lamaze, 2002). Moreover, this endocytic route has been
481 previously emphasized for TiONts internalization in cardiomyocytes (Papa *et al.*, 2013).
482 Since the nanotubes elaborated in this study are agglomerated with sizes higher than
483 several hundreds of nanometers (see Figure 7), macropinocytosis seems to be relevant.
484 Moreover, the presence of nanoparticles in contact with microglial cells may induce a
485 change in mitochondria location and size which can be explained by changes in
486 mitochondrial activity, however no change in cell size or morphology is observed.

487 Particles taken up by the cells ultimately fuse with lysosomes. Lysosomal
488 membrane permeabilization (LMP) is one of the factors contributing to metal oxide
489 nanoparticles toxicity (Sabella *et al.*, 2014). In this work TiONts-APTES nanoparticles
490 do not induce LMP in BV-2 cells as it is indicated by the unaltered intensity of AO
491 signal.

492 ROS production is an important factor contributing to nanoparticle mediated
493 toxicity. In the present study, BV-2 cells exhibit dose dependent increase in superoxide
494 anion production after 6 h which get normalized by 24 h. On the other hand, the level of
495 peroxide radicals remains similar across all experiment groups for 6h which get
496 elevated in a dose dependent manner for 24 h. This time-dependent increase in peroxide
497 radicals may be due to the delayed induction of superoxide dismutase which carries out
498 the enzymatic conversion of superoxide radicals. Microglia in response to toxic signals
499 may undergo an oxidative burst. This can be monitored by the immediate rise in
500 superoxide radicals which ultimately get converted into peroxide radicals (Long *et al.*,
501 2006). The results obtained in this work are in concordance with the aforementioned
502 findings.

503 BV-2 cells exposed to TiONts-APTES exhibit an increase in $\Delta\Psi m$ 6 h after
504 incubation. Hyperpolarization is an early and reversible event in immune cell activation

and apoptosis (Perl *et al.*, 2004). Oxidative burst and mitochondrial hyperpolarization point to the chance of TiONts-APTES mediated microglial activation in cells. Microglial activation is characterized by increased cell proliferation, altered morphology and increase in the cell size (Block and Hong, 2007). To examine microglial activation potential of TiONts-APTES, cell cycle analysis is carried out. No sign of cell cycle alterations is observed in TiONts-APTES exposed cells. Normal 'S' phase in treated cells confirms the absence of increased DNA synthesis in BV-2 cells. On the other hand, cytotoxic agent 7-kc cholesterol induces a significant reduction in S and G2-M phases with a corresponding increase in Sub G1 (apoptotic) population. The morphological analysis further supports these findings where no change in morphology, cell size or cell density is observed in BV-2 cells exposed to TiONts-APTES suggesting their low cytotoxicity.

Nanoparticle-mediated cell death can occur *via* the two main types of cell death: apoptosis and necrosis (Hirsch *et al.*, 1998). To study the mechanism of TiONts-APTES mediated cell death, the PARP cleavage assay is carried out. PARP cleavage is a marker for apoptotic mode of cell death and is mediated by suicidal proteases like caspases and cathepsin (Boya and Kroemer, 2008). TiONts-APTES exposure induced PARP cleavage in BV-2 cells. Studies show that lysosomal proteases are probably involved in nanoparticles toxicity (Sruthi and Mohanan, 2016). To evaluate whether the PARP cleavage is influenced by the lysosomal proteases (cathepsin), cells are pre-treated with a cathepsin inhibitor Z-FA-FMK. In contrary to the expectation, the cathepsin inhibitor, which also induces PARP fragmentation, does not attenuate PARP cleavage in BV-2 cells. The result of the PARP cleavage suggests a potential activation of an apoptotic mode of cell death in TiONts-APTES exposed BV-2 cells.

The analysis of plasma membrane integrity further confirms the apoptotic mode of cell death. The loss of plasma membrane integrity occurs in the late phase of apoptosis. Cells at the early stage of apoptosis possess intact membrane. Absence of PI positive cells in the population after 24 h of TiONts-APTES incubation further supported TiONts-APTES mediated apoptosis in BV-2 cells. Moreover, it suggests that BV-2 cells are probably at their early stage of apoptosis at 24 h of treatment.

Conclusion

Safety and toxicity are major concerns when it comes to biomedical applications of nanoparticles. In the present study, bio-interaction of APTES-functionalized TiONts were carried out using BV-2 microglial cells. Despite the changes in mitochondrial activity and ROS production, no morphological variation or plasma membrane permeability alteration was observed in cells exposed to TiONts-APTES. These results were confirmed by TEM images that showed a normal cellular morphology after TiONts-APTES uptake and changes in mitochondria location and size. The particles induced an initial increase in transmembrane mitochondrial potential ($\Delta\Psi m$) which reverted to normal state by 24 h. TiONts-APTES do not interfere with lysosomal membrane integrity or cell cycle. Caspase-dependent apoptosis probably mediates the toxicity. The time- and dose-dependent toxicity is obvious only at the highest concentration used (80 µg/mL). It is shown through TEM images that the main process of nanoparticles internalization in BV-2 cells is endocytosis. These cells do not show any sign of activation which is a major hurdle in drug delivery applications across brain. This study proves that APTES-functionalized TiONts are a potential candidate for drug delivery applications across the brain.

Acknowledgments

The authors thank the Director and the Head, Bio Medical Technology Wing, Sree Chitra Tirunal Institute for Medical Sciences and Technology, Thiruvananthapuram for providing the infrastructure. Sruthi S thanks, University Grants Commission, New Delhi and Indo-French Centre for the Promotion of Advanced Research, New Delhi for the Junior Research Fellowship and the Raman-Charpak Fellowship. The authors are also grateful to Thomas Nury for his expertise in flow cytometry and western blot analysis, to Dr. Olivier Heintz for XPS measurements and to Dr. Rémi Chassagnon for TEM observations. This work was also possible with help from CellImaP / Dimacell core facility of the University of Burgundy, especially Amandine Bataille for electron microscopy. The core facility is supported by the following institutions: Conseil Régional Bourgogne Franche-Comté through the “Plan d'Actions Régional pour l'Innovation (PARI)” and the European Union through the PO FEDER-FSE Bourgogne 2014/2020 programs.

Declaration of interest

The authors report no conflicts of interest.

References

Bavykin, D.V., Walsh, F.C., 2010. Titanate and titania nanotubes: synthesis, properties and applications, in: Cambridge, UK, Royal Society of Chemisty, 154 pp.

Benmerah, A., Lamaze, C., 2002. Multiple endocytic pathways in mammalian cells. Med. Sci., 18, 1126–1136.

574 Blasi, E., Barluzzi, R., Bocchini, V., Mazzolla, R., Bistoni, F., 1990. Immortalization of
575 murine microglial cells by a v-raf/v-myc carrying retrovirus. J. Neuroimmunol.,
576 27, 229–237.
577 Block, M., Hong, J.S., 2007. Chronic microglial activation and progressive
578 dopaminergic neurotoxicity. Biochem. Soc. Trans., 35, 1127-1132.
579 Boudon, J., Papa, A., Paris, J., Millot, N., 2014. Titanate nanotubes as a versatile
580 platform for nanomedicine, in: Nanomedicine, Seifalian, A., De Mel, A.,
581 Kalaskar, D.M., One Central Press (OCP), pp.403-428.
582 Boya, P., Kroemer, G., 2008. Lysosomal membrane permeabilization in cell death.
583 *Oncog.*, 27, 6434–6451.
584 Bussy, C., Al-Jamal, K.T., Boczkowski, J., Lanone, S., Prato, M., Bianco, A.,
585 Kostarelos, K., 2015. Microglia determine brain region-specific neurotoxic
586 responses to chemically functionalized carbon nanotubes. *ACS nano,* 9, 7815–
587 7830.
588 Chen, J., Zhou, H., Santulli, A.C., Wong, S.S., 2010. Evaluating cytotoxicity and
589 cellular uptake from the presence of variously processed TiO_2 nanostructured
590 morphologies. *Chem. Res. Toxicol.,* 23, 871–879.
591 Hirsch, T., Susin, S., Marzo, I., Marchetti, P., Zamzami, N., Kroemer, G., 1998.
592 Mitochondrial permeability transition in apoptosis and necrosis. *Cell Biol.*
593 *Toxicol.,* 14, 141–145.
594 Huerta-García, E., Márquez-Ramírez, S.G., del Pilar Ramos-Godinez, M., López-
595 Saavedra, A., Herrera, L.A., Parra, A., Alfaro-Moreno, E., Gómez, E.O., López-
596 Marure, R., 2015. Internalization of titanium dioxide nanoparticles by glial cells
597 is given at short times and is mainly mediated by actin reorganization-dependent
598 endocytosis. Neurotoxicol., 51, 27–37.

599 Iavicoli, I., Leso, V., Fontana, L., Bergamaschi, A., 2011. Toxicological effects of
600 titanium dioxide nanoparticles: a review of in vitro mammalian studies. Eur.
601 Rev. Med. Pharmacol. Sci., 15, 481–508.
602 Kasuga, T., Hiramatsu, M., Hoson, A., Sekino, T., Niihara, K., 1998. Formation of
603 titanium oxide nanotube. Langmuir, 14, 3160–3163.
604 Kessler, R., 2011. Engineered nanoparticles in consumer products: understanding a new
605 ingredient. Environ. Health Perspect., 119, A120–A125.
606 Kijima, T., 2010. Inorganic and Metallic Nanotubular Materials: Recent Technologies
607 and Applications, in: Kijima, T. (Eds), Springer-Verlag Berlin Heidelberg.
608 Lizard, G., Fournel, S., Genestier, L., Dhedin, N., Chaput, C., Flacher, M., Mutin, M.,
609 Panaye, G., Revillard, J.P., 1995. Kinetics of plasma membrane and
610 mitochondrial alterations in cells undergoing apoptosis. Cytometry A, 21, 275–
611 283.
612 Loiseau, A., Boudon, J., Mirjolet, C., Crehange, G., Millot, N., 2017. Taxane-Grafted
613 Metal-Oxide Nanoparticles as a New Theranostic Tool against Cancer: The
614 Promising Example of Docetaxel-Functionalized Titanate Nanotubes on Prostate
615 Tumors. Adv. Healthc. Mater. 6 (16), 1700245.
616 Long, T.C., Saleh, N., Tilton, R.D., Lowry, G.V., Veronesi, B., 2006. Titanium dioxide
617 (P25) produces reactive oxygen species in immortalized brain microglia (BV-2):
618 implications for nanoparticle neurotoxicity. Environ. Sci. Technol., 40, 4346–
619 4352.
620 Lupu, A., Popescu, T., 2013. The noncellular reduction of MTT tetrazolium salt by
621 TiO_2 nanoparticles and its implications for cytotoxicity assays. Toxicol. In Vitro,
622 27, 1445–1450.

623 Marel, A.K., Lizard, G., Izard, J.C., Latruffe, N., Delmas, D., 2008. Inhibitory effects of
624 trans-resveratrol analogs molecules on the proliferation and the cell cycle
625 progression of human colon tumoral cells. Mol. Nutr. Food Res., 52, 538–548.
626 Mirjolet, C., Boudon, J., Loiseau, A., Chevrier, S., Boidot, R., Oudot, A., Collin, B.,
627 Martin, E., Joy, P.A., Millot, N., 2017. Docetaxel-titanate nanotubes enhance
628 radiosensitivity in an androgen-independent prostate cancer model. Int. J.
629 Nanomed., 12, 6357-6363.
630 Mirjolet, C., Papa, A., Créhange, G., Raguin, O., Seignez, C., Paul, C., Truc, G.,
631 Maingon, P., Millot, N., 2013. The radiosensitization effect of titanate nanotubes
632 as a new tool in radiation therapy for glioblastoma: a proof-of-concept.
633 Radiother. Oncol., 108, 136–142.
634 Niu, L., Shao, M., Wang, S., Lu, L., Gao, H. & Wang, J., 2008. Titanate nanotubes:
635 preparation, characterization, and application in the detection of dopamine. J.
636 Mater. Sci., 43, 1510–1514.
637 Nury, T., Zarrouk, A., Ragot, K., Debbabi, M., Riedinger, J.-M., Vejux, A., Aubourg,
638 P., Lizard, G., 2017. 7-Ketocholesterol is increased in the plasma of X-ALD
639 patients and induces peroxisomal modifications in microglial cells: Potential
640 roles of 7-ketocholesterol in the pathophysiology of X-ALD. J. Steroid
641 Biochem. Mol. Biol., 169, 123–136.
642 Ormerod, M.G., Collins, M.K., Rodriguez-Tarduchy, G., Robertson, D., 1992.
643 Apoptosis in interleukin-3-dependent haemopoietic cells: Quantification by two
644 flow cytometric methods. J. Immunol. Methods, 153, 57–65.
645 Papa, A.-L., Boudon, J., Bellat, V., Loiseau, A., Bisht, H., Sallem, F., Chassagnon, R.,
646 Bérard, V., Millot, N., 2015. Dispersion of titanate nanotubes for nanomedicine:
647 comparison of PEI and PEG nanohybrids. Dalton Trans., 44, 739–746.

Papa, A.-L., Maurizi, L., Vandroux, D., Walker, P., Millot, N., 2011. Synthesis of Titanate Nanotubes Directly Coated with USPIO in Hydrothermal Conditions: A New Detectable Nanocarrier. J. Phys. Chem. C, 115**,** 19012–19017.

Papa, A.-L., Millot, N., Saviot, L., Chassagnon, R., Heintz, O., 2009. Effect of Reaction Parameters on Composition and Morphology of Titanate Nanomaterials. J. Phys. Chem. C, 113, 12682–12689.

Papa, A.L., Dumont, L., Vandroux, D., Millot, N., 2013. Titanate nanotubes: towards a novel and safer nanovector for cardiomyocytes. Nanotoxicology, 7, 1131–42.

Paris, J., Bernhard, Y., Boudon, J., Heintz, O., Millot, N., Decréau, R.A., 2015. Phthalocyanine-titanate nanotubes: a promising nanocarrier detectable by optical imaging in the so-called imaging window. RSC Adv., 5, 6315–6322.

Perl, A., Gergely, P., Nagy, G., Koncz, A., Banki, K., 2004. Mitochondrial hyperpolarization: a checkpoint of T-cell life, death and autoimmunity. Trends Immunol., 25, 360–367.

Pierzyńska-Mach, A., Janowski, P.A., Dobrucki, J.W., 2014. Evaluation of acridine orange, LysoTracker Red, and quinacrine as fluorescent probes for long-term tracking of acidic vesicles. Cytometry A, 85, 729–737.

Quent, V., Loessner, D., Friis, T., Reichert, J.C., Hutmacher, D.W., 2010. Discrepancies between metabolic activity and DNA content as tool to assess cell proliferation in cancer research. J. Cell. Mol. Med., 14, 1003–1013.

Rehman, F., Zhao, C., Jiang, H., Wang, X., 2016. Biomedical applications of nano-titania in theranostics and photodynamic therapy. Biomater. Sci., 4, 40–54.

Rihane, N., Nury, T., M'rad, I., Mir, L., Sakly, M., Amara, S., Lizard, G., 2016. Microglial cells (BV-2) internalize titanium dioxide (TiO_2). Environ. Sci. Pollut. Res. Int., 23, 9690–9699.

673 Riss, T.L., Moravec, R.A., Niles, A.L., Duellman, S., Benink, H.A., Worzella, T.J.,
674 Minor, L., 2013 (updated 2016). Cell viability assays, in: Sittampalam, G.S.,
675 Coussens, N.P., Brimacombe, K., *et al.*, editors. Assay Guidance Manual
676 [Internet]. Bethesda (MD): Eli Lilly & Company and the National Center for
677 Advancing Translational Sciences; 2004-. Available from:
678 https://www.ncbi.nlm.nih.gov/books/NBK144065/
679 Sabella, S., Carney, R.P., Brunetti, V., Malvindi, M.A., Al-Juffali, N., Vecchio, G.,
680 Janes, S.M., Bakr, O.M., Cingolani, R., Stellacci, F., 2014. A general
681 mechanism for intracellular toxicity of metal-containing nanoparticles.
682 Nanoscale, 6, 7052–7061.
683 Sabzi, M., Mirabedini, S.M., Zohuriaan-Mehr, J., Atai, M., 2009. Surface modification
684 of TiO_2 nano-particles with silane coupling agent and investigation of its effect
685 on the properties of polyurethane composite coating. Prog. Org. Coat., 65, 222–
686 228.
687 Sallem, F., Boudon, J., Heintz, O., Séverin, I., Megriche, A., Millot, N., 2017. Synthesis
688 and characterization of chitosan-coated titanate nanotubes: towards a new safe
689 nanocarrier. Dalton Trans.. 46, 15386–15398
690 Saquib, Q., Al-Khedhairy, A.A., Siddiqui, M.A., Abou-Tarboush, F.M., Azam, A.,
691 Musarrat, J., 2012. Titanium dioxide nanoparticles induced cytotoxicity,
692 oxidative stress and DNA damage in human amnion epithelial (WISH) cells.
693 Toxicol. in Vitro, 26, 351–361.
694 Sruthi, S., Mohanan, P., 2016. Engineered zinc oxide nanoparticles; biological
695 interactions at the organ level. Curr. Med. Chem., 23, 1–12.

696 Suzuki, H., Toyooka, T., Ibuki, Y., 2007. Simple and easy method to evaluate uptake
697 potential of nanoparticles in mammalian cells using a flow cytometric light
698 scatter analysis. Environ. Sci. Technol., 41, 3018–3024.

699

700

Tables

	Starting degradation temperature (°C)	Mass loss (%)	Degraded molecular weight ($g.mol^{-1}$)	Molecule.nm^{-2}
TiONts	175	2.8	18	(10.6 ± 1.5) OH, n=10
TiONts-APTES	160	10.3	58	(7.3 ± 0.5) APTES, n=7

Table 1. Results of mass loss and hydroxyl groups density and grafting ratio of bare TiONts and TiONts-APTES respectively (n is the number of syntheses realized before pooling the different batches, they allow to evaluate the reproducibility of our syntheses).

Atomic concentration (%)	C_{1s}	O_{1s}	Na_{KLL}	Ti_{2p}	N_{1s}	Si_{2p}
TiONts	7.3	58.7	13.5	20.5	-	-
% Elements TiONts / Ti	0.3	2.9	0.7	1.0	-	-
TiONts-APTES	11.2	56.8	5.7	21.5	2.3	2.5
% Elements TiONts-APTES / Ti	0.5	2.6	0.3	1.0	0.1	0.1

Table 2. XPS elemental analyses and their corresponding ratio to titanium of bare TiONts and TiONts-APTES.

Figures

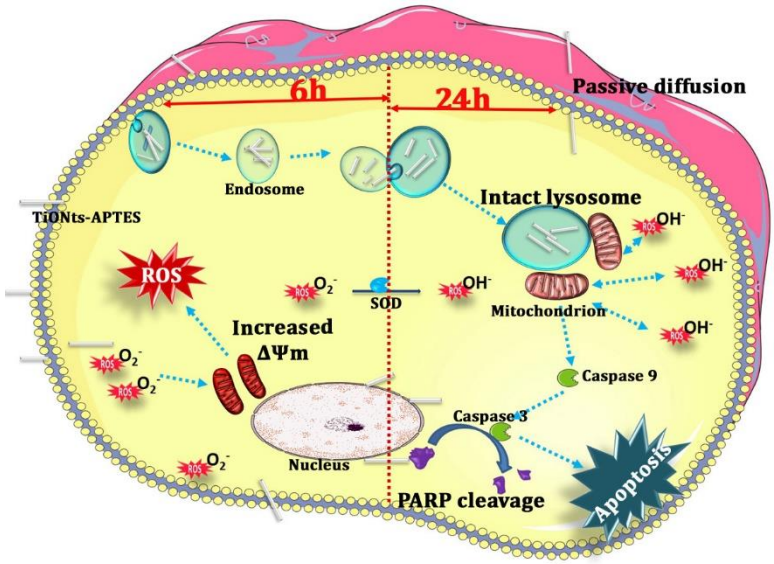

Graphical abstract: (3-aminopropyl) triethoxysilane (APTES) functionalized titanate nanotubes (named TiONts on the scheme) enter the BV-2 cell both *via* endocytosis and passive diffusion. Inside cell, TiONts-APTES are capable of inducing superoxide radicals which later get converted to peroxides by SOD activity. TiONts-APTES interact with mitochondria to induce a transient increase in ΔΨm which further gives way to mitochondria mediated ROS production. TiONts-APTES do not affect lysosomal integrity or cell cycle pattern. At high concentration TiONts-APTES probably induce caspase-mediated apoptosis in BV-2 cells leading to PARP cleavage.

721 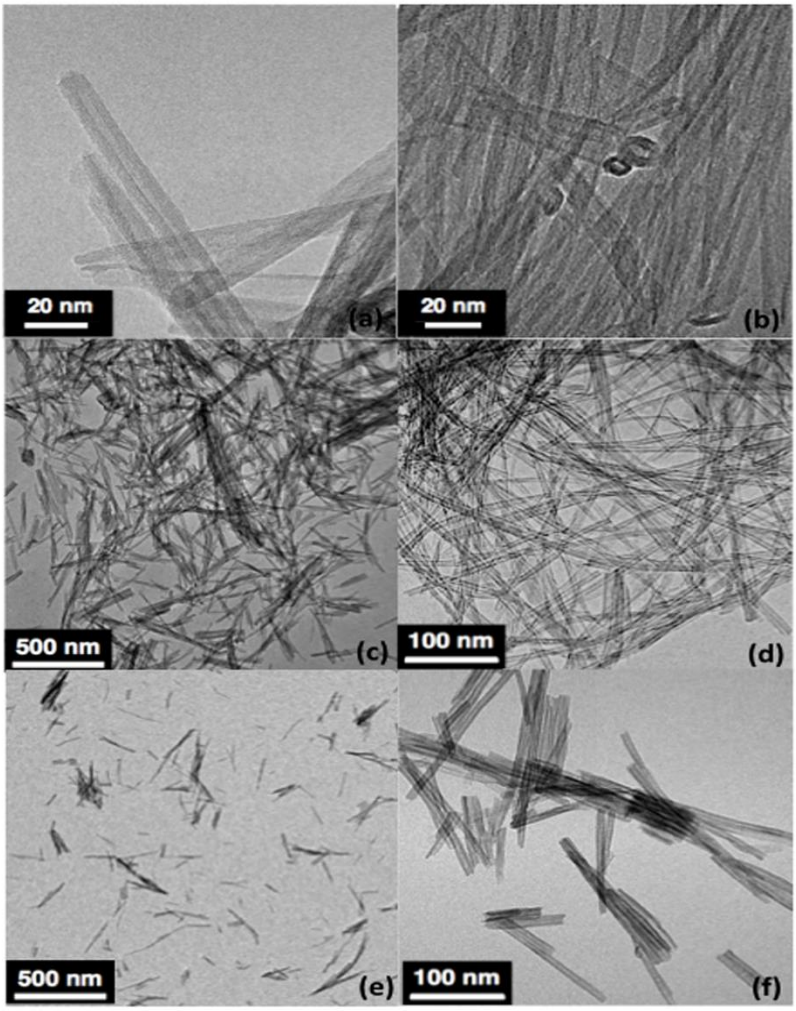

722 Figure 1. TEM images highlight (a-b) the formation of bare TiONts and the evolution of

723 TiONts dispersion (c-d) before and (e-f) after APTES grafting.

724

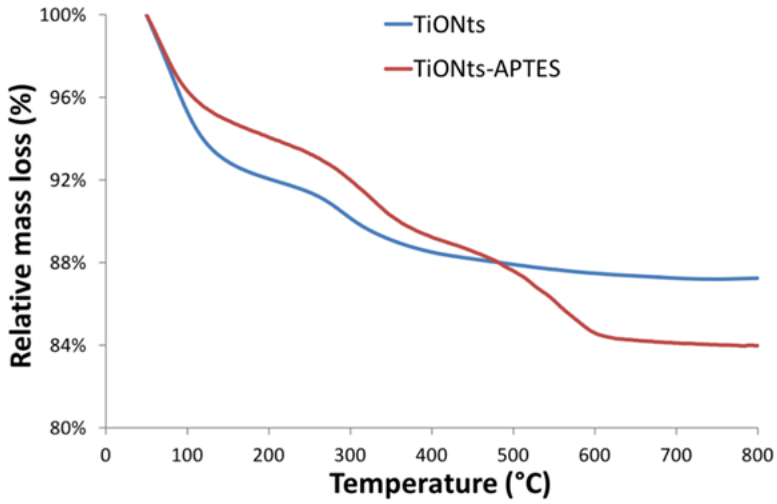

Figure 2. TGA curves of bare TiONts and TiONts-APTES under air atmosphere.

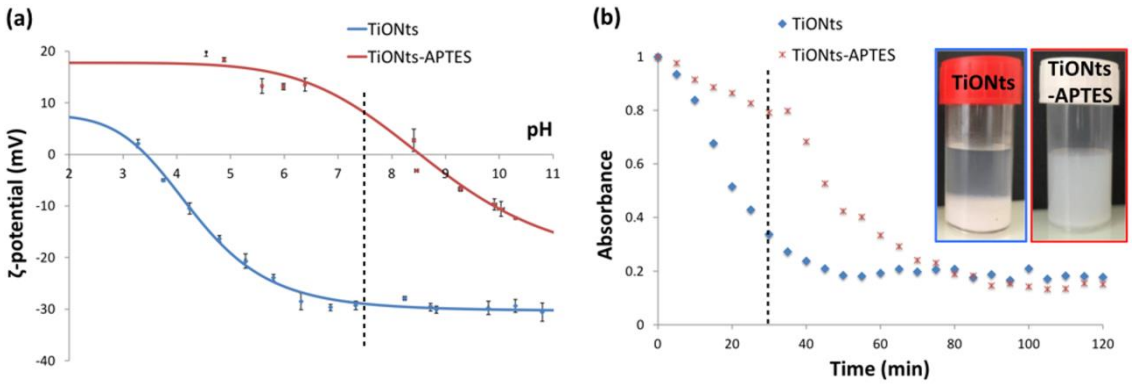

Figure 3. (a) ζ potential curves of bare TiONts and TiONts-APTES (the vertical dashed line corresponds to the physiological pH). (b) Colloidal stability of bare TiONts and TiONts-APTES (PBS 0.1 M; pH 7.4) over 120 min following their absorbance at 600 nm by turbidimetry. The pictures of TiONts (left) and TiONts-APTES (right) suspensions in PBS (0.1 M; pH 7.4) correspond to the vertical dashed line at 30 min.

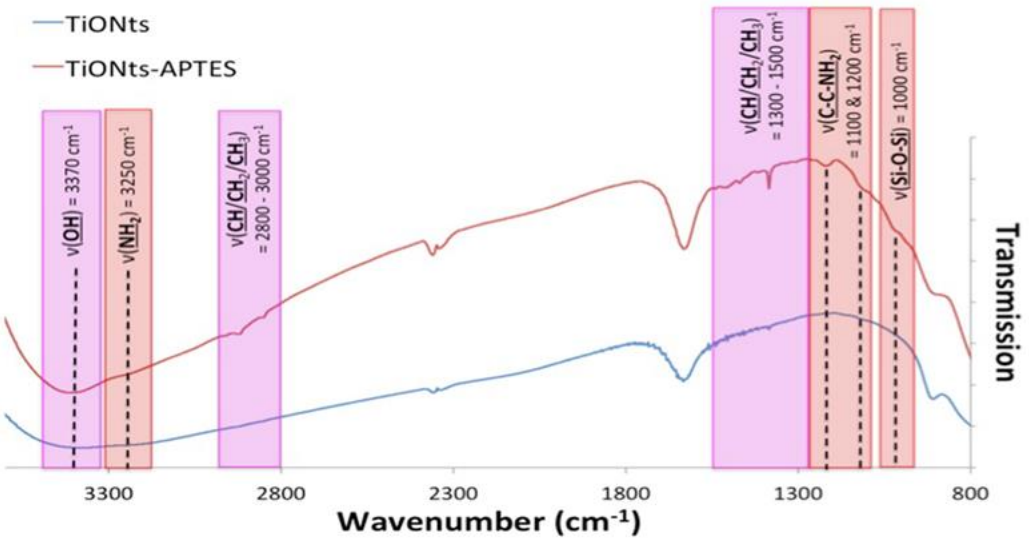

735

736 Figure 4. FT-IR spectra of bare TiONts and TiONts-APTES. Red vibrational bands
737 highlight the presence of APTES on the surface of TiONts.

738

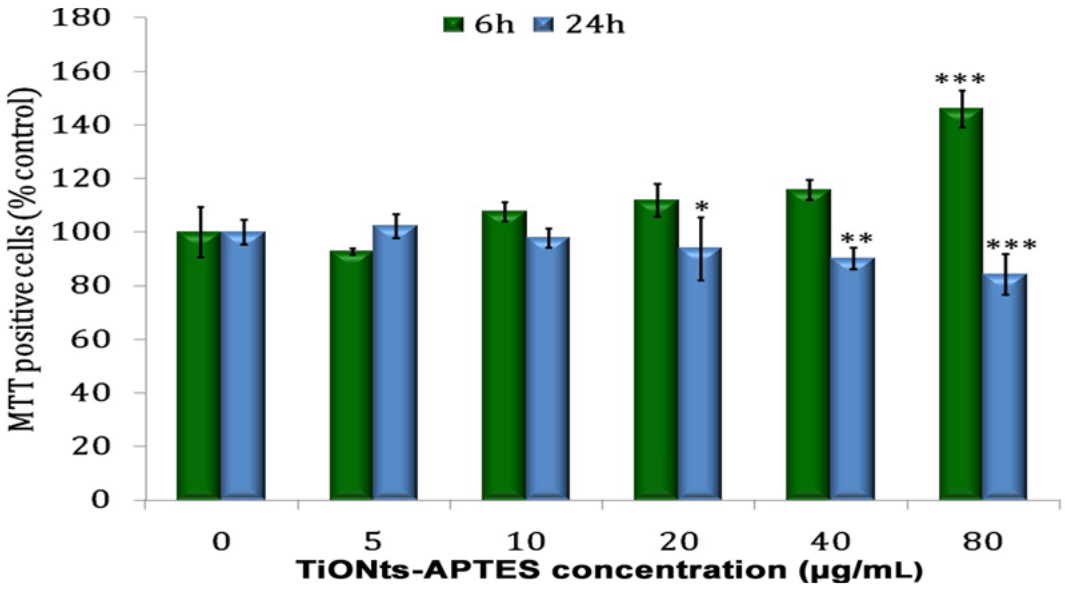

739

740 Figure 5. (a) Dose response and cytotoxicity in BV-2 cells exposed to TiONts-APTES
741 for 6 and 24 h indicated by percentage MTT positive cells. Data represents mean ± SD
742 of three independent experiments. Asterisks denote statistically significant differences
743 compared to the control (* $p<0.05$, ** $p< 0.01$ and *** $p<0.001$).

744

745

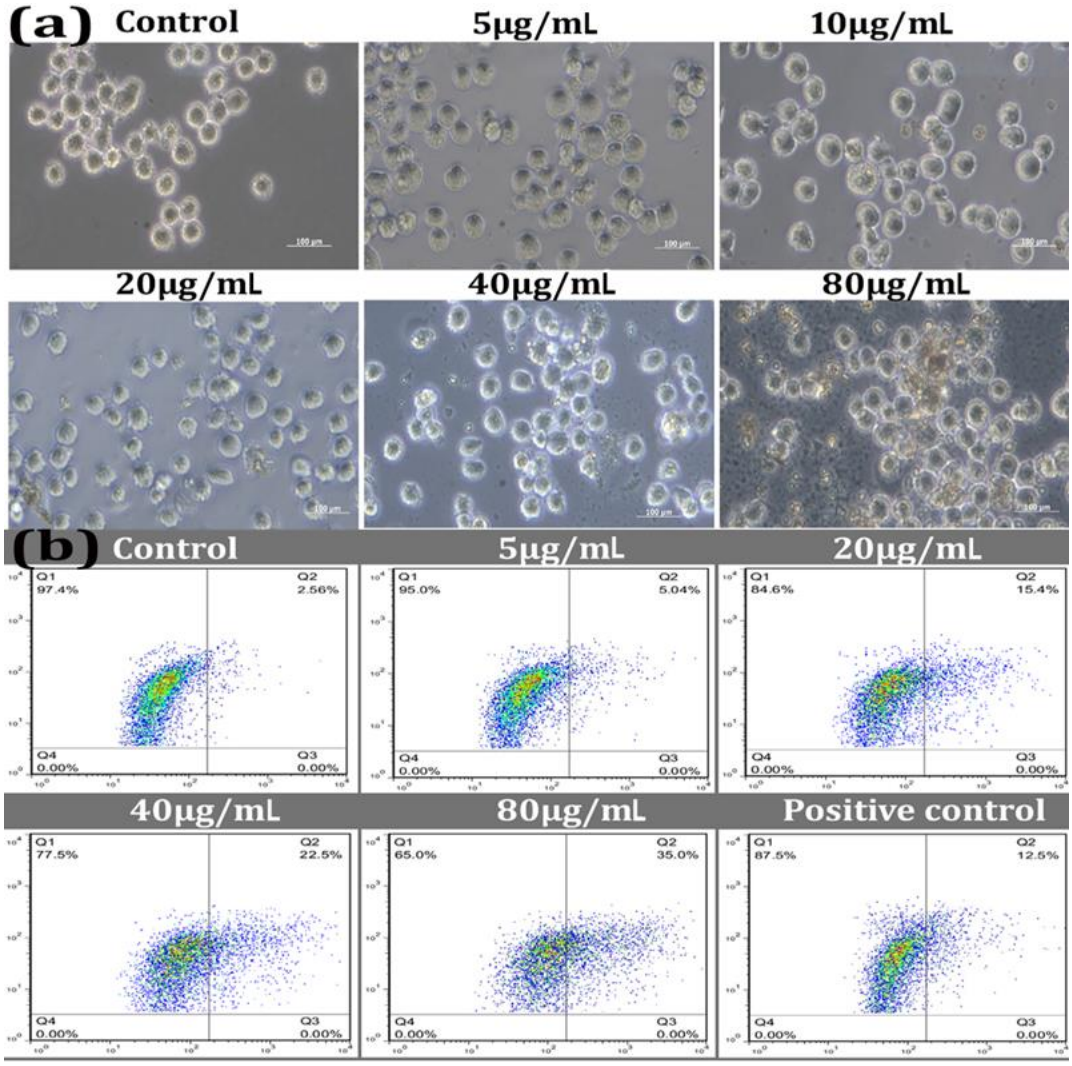

746

747 Figure 6. (a) Cell morphology analysis of BV-2 cells exposed to TiONts-APTES for
748 24 h. Scale bar represents 100 µm. As the highest concentration used the nanoparticles
749 sediments could be observed. (b) Cellular uptake of TiONts-APTES by BV-2 cells:
750 cells were exposed to TiONts-APTES for 6 h and the increase in side scatter (SSC) with
751 respect to forward scatter (FSC) was measured. 7-ketocholesterol-treated cells were
752 used as positive control. All the cellular debris were gated out to represent the data.

753

754

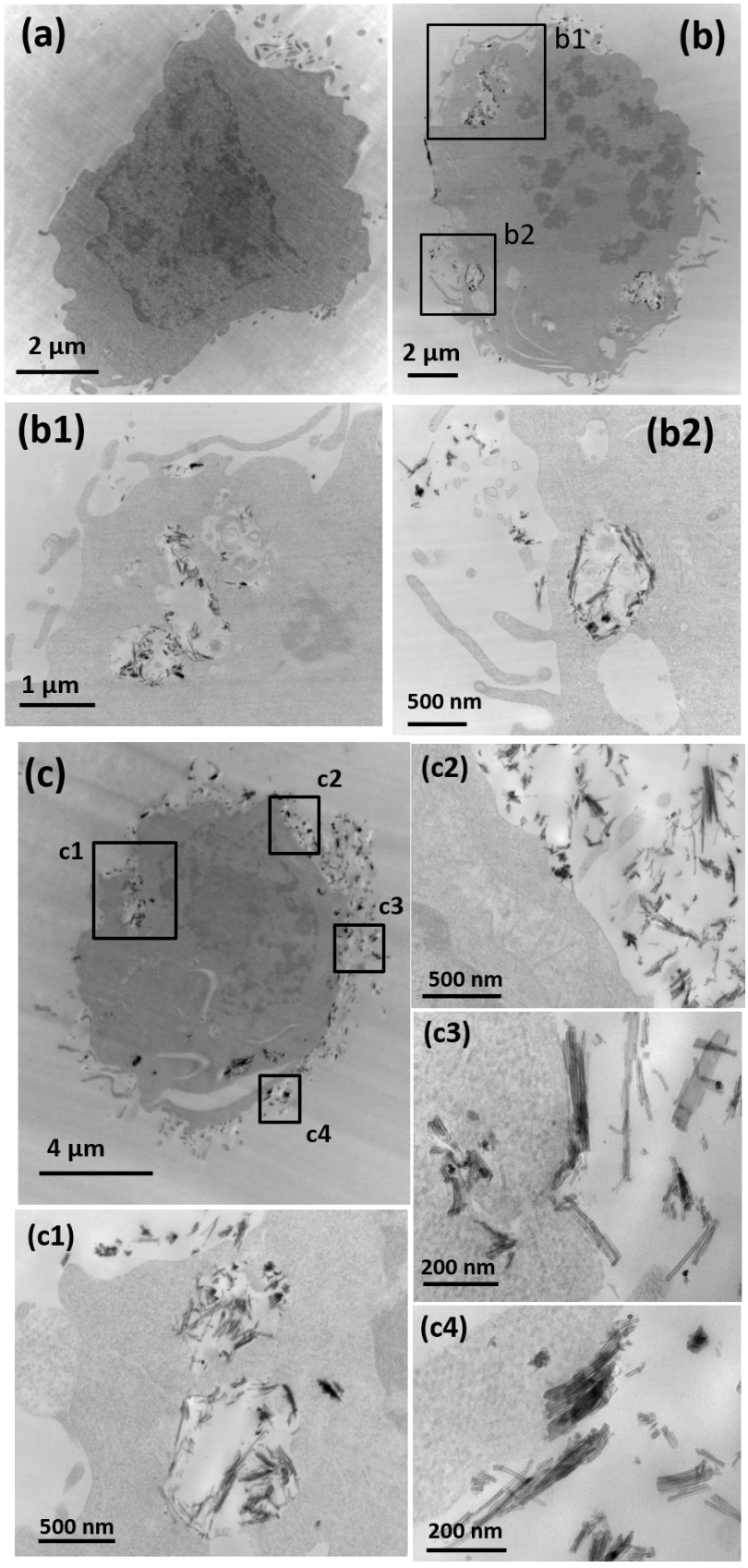
(a)
2 µm
(b)
b1
b2
2 µm
(b1)
1 µm
(b2)
500 nm
(c)
c1
c2
c3
c4
4 µm
(c1)
500 nm
(c2)
500 nm
(c3)
200 nm
(c4)
200 nm

755

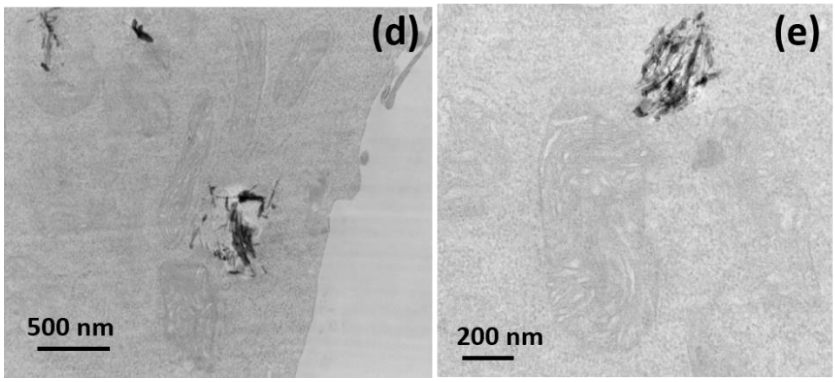

Figure 7 : TEM images of (a) BV-2 control cells, (b,b1,b2) BV-2 cells treated with 20 µg/mL of TiONts-APTES without amiloride (c,c1,c2,c3,c4) BV-2 cells treated with 20 µg/mL of TiONts-APTES and 100µM of amiloride, incubated for 24 h (d) endocytosis vesicle surrounded by four mitochondria (e) endocytosis vesicle in contact with mitochondria.

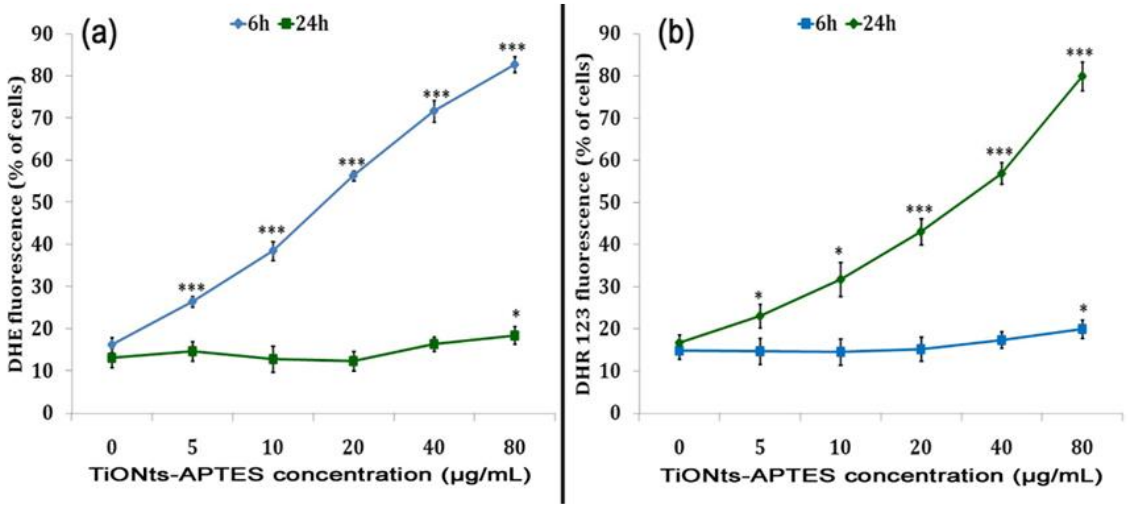

Figure 8. ROS generation in BV-2 cells exposed to TiONts-APTES for 6 and 24 h. (a) Superoxide radical formation (b), hydrogen peroxide radical formation. Data represents mean ±SD of three independent experiments. Asterisks denote statistically significant differences compared to control (* $p<0.05$, ** $p< 0.01$ and *** $p<0.001$).

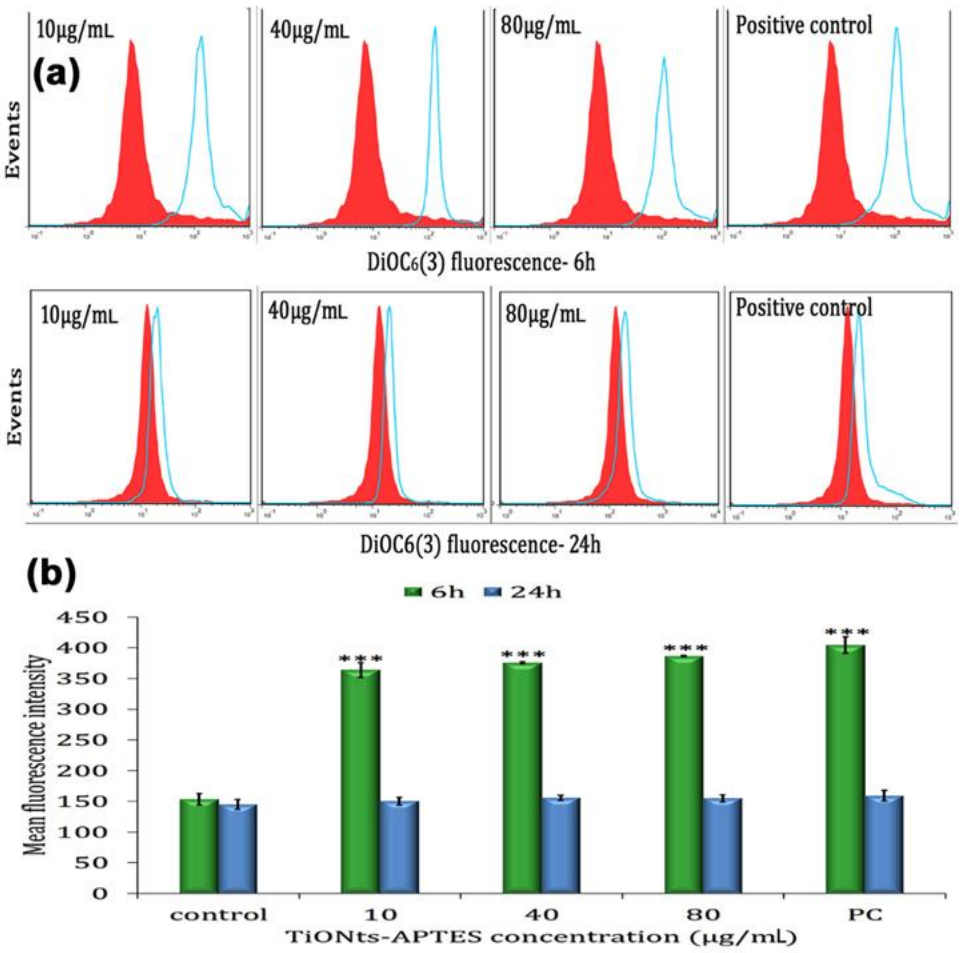

Figure 9. (a) Transmembrane mitochondrial potential in BV-2 cells exposed to TiONts-APTES at 6 and 24 h. Cells incubated with 4% paraformaldehyde were used as positive control (PC). Red solid peaks represent $DiOC_6(3)$ intensity of untreated control while blue tinted peaks represent treated groups. The gated population includes both dead and viable cells. (b) Flow cytometric quantification of transmembrane mitochondrial potential ($\Delta\Psi m$). Data shown represent mean ± SD of three independent experiments. Asterisks denote statistically significant differences compared to control (*** p value <0.001).

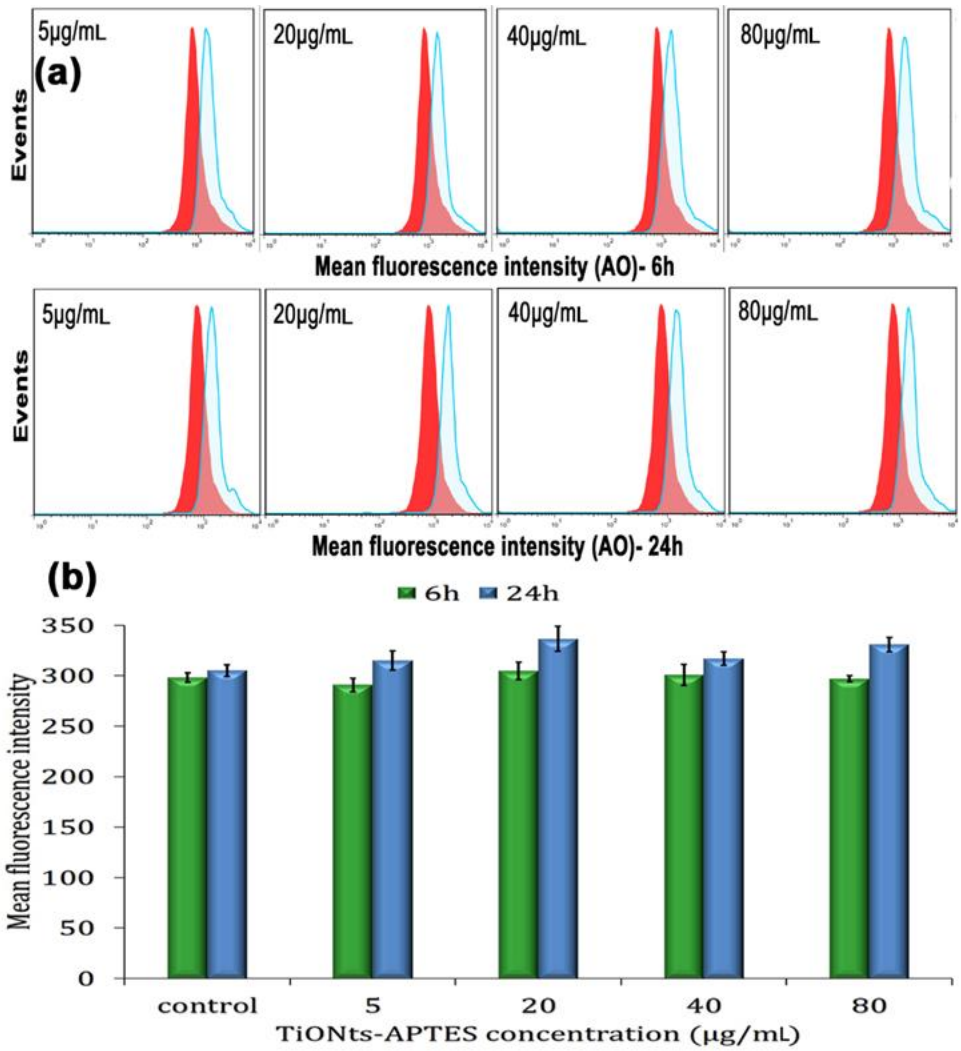

779

780 Figure 10. (a) Lysosomal membrane integrity of BV-2 cells exposed to TiONts-APTES
781 for 6 and 24 h. The red solid peaks denote AO intensity in control population while blue
782 tinted peaks represent treatment groups. The gated population includes both viable and
783 dead cells. (b) Flow cytometric quantification of the lysosomal membrane integrity.
784 Data shown represent mean ± SD of three independent experiments.

785

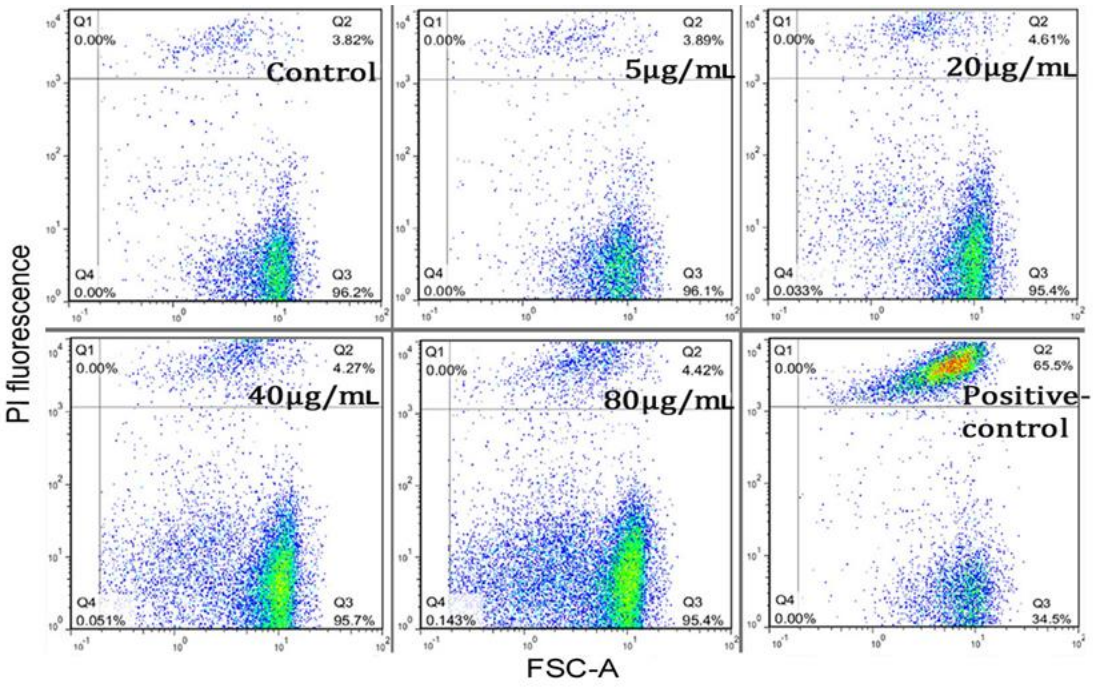

786

787 Figure 11. Plasma membrane integrity in BV-2 cells exposed to TiONts-APTES for 24
788 h. 7-ketocholesterol treated cells were used as positive control. The gating was done
789 with respect to PI fluorescence of positive control. Gated population includes both live
790 and dead cells. n = 3.

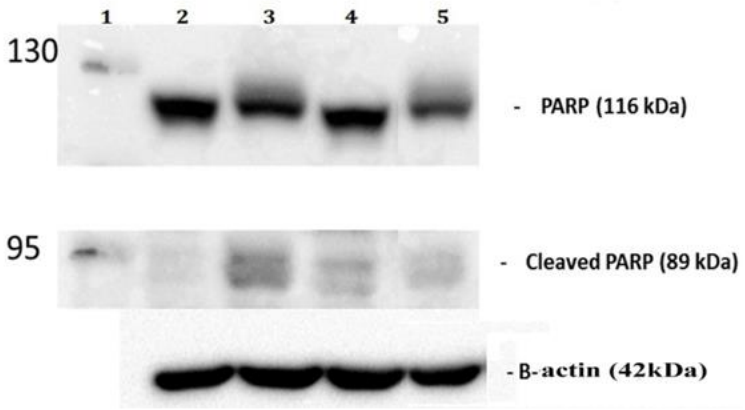

791

792 Figure 12. PARP cleavage assay in BV-2 cells exposed to TiONts-APTES for 24 h.
793 Lane 1: protein marker, Lane 2: control cells, Lane3: control cells pre-treated with Z-
794 Fa-FMK, lane 4: TiONts-APTES (80 µg/mL), lane 5: 80 µg/mL TiONts-APTES pre-
795 treated with Z-Fa-FMK.

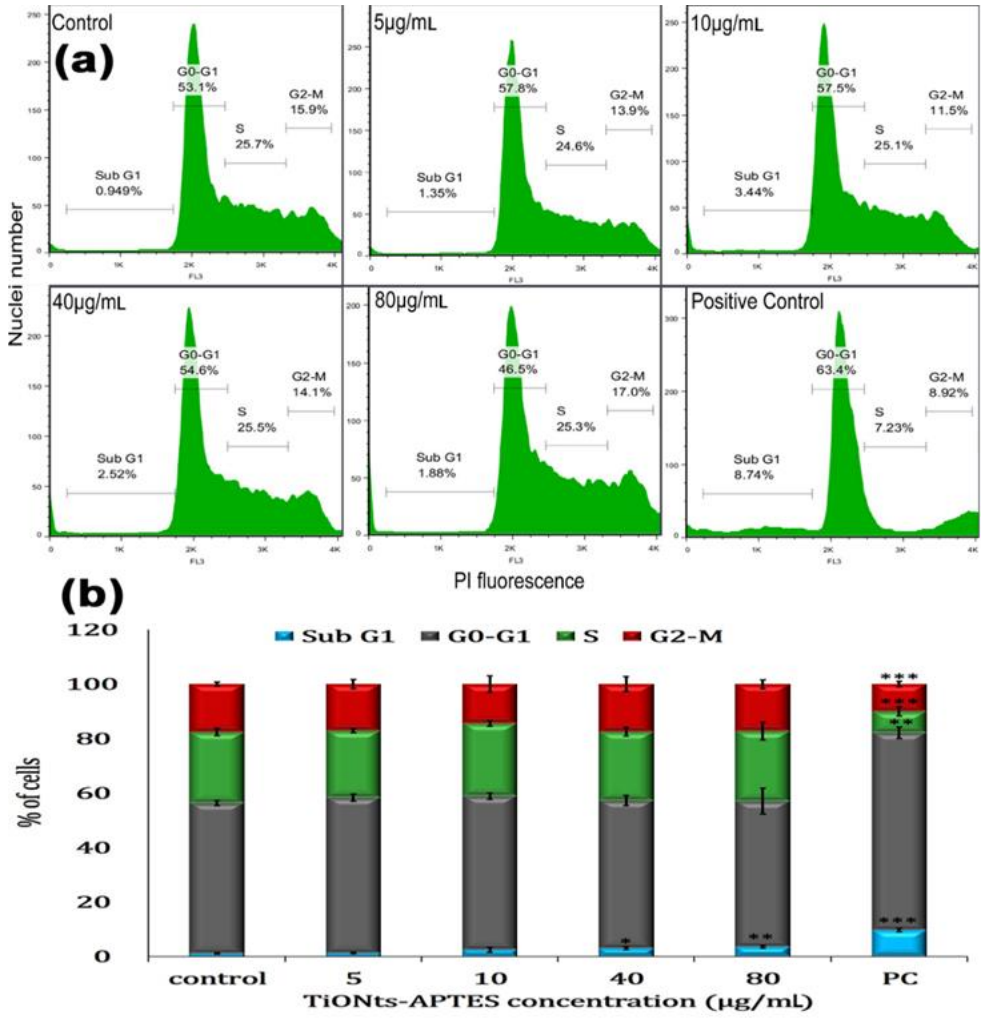

796

797 Figure 13. (a) Cell cycle analysis of BV-2 cells exposed to TiONts-APTES for 24 h. (b)
798 quantification of the cell cycle analysis. 7-ketocholestrol-treated cells were used as
799 positive control (PC). All the cellular debris has been gated out to represent the data.
800 Data shown represent mean ± SD of three independent experiments. Asterisks denote
801 statistically significant differences compared to control (* p value <0.05, ** p value <
802 0.01 and *** p value <0.001).

803